Available online at www.sciencedirect.com
SCIENCE DIRECT®
PERGAMON
International Journal of Heat and Mass Transfer 46 (2003) 4453–4466
International Journal of HEAT and MASS TRANSFER
www.elsevier.com/locate/ijhmt

Local condensation heat transfer rates in fine passages

J.R. Baird, D.F. Fletcher, B.S. Haynes *

Department of Chemical Engineering, University of Sydney, Sydney, NSW 2006, Australia

Received 10 January 2003; received in revised form 25 April 2003

Abstract

A novel apparatus capable of quantitative control of local heat flows to single fine passages through thermoelectric coolers has been developed. Local heat transfer coefficients for flow condensation of HCFC-123 and of R11 have been measured for a wide range of mass fluxes (70–600 $\mathrm{kg\,m^{-2}\,s^{-1}}$), heat fluxes (15–110 $\mathrm{kW\,m^{-2}}$), vapour qualities (superheated to fully condensed), and pressures (120–410 kPa) in tubes with internal diameters of 0.92 and 1.95 mm. The data show a strong influence of mass flux and local quality on the heat transfer coefficient, with a weaker influence of system pressure. The data also show a clear enhancing effect of the condensation rate (heat flux) on the heat transfer coefficient. There is very little influence of tube diameter over the range investigated.

A simple model of gas–liquid shear-driven annular flows, with a turbulent liquid film and allowance for the influence of condensation rates on the gas–liquid interfacial shear force, accounts quantitatively for the major effects observed. An average overprediction of 5% is obtained for the data set of more than 2000 points, with a standard deviation of 25%. However, the model does not predict the full extent of the observed effect of condensation rate on the heat transfer coefficients and some improvement in the description of the interfacial shear force is apparently needed.

Keywords: Narrow passage; Condensation heat transfer; Microchannel; Microtube

1. Introduction

With growing interest in the use of fine passages for microreaction technology and more generally for highly compact heat transfer applications, there is an increasing need for better understanding of heat transfer phenomena in such systems. As reviewed recently by Palm [1], while single-phase flows and flow boiling have received considerable attention in the past 10 years, there remains a dearth of information on condensation in narrow tubes. Here we take narrow tubes to include hydraulic mean diameters of less than a few mm.

Webb and coworkers [2–6] have reported a series of measurements on condensation of R12 and R134a in small-diameter extruded multiport channels. They have studied hydraulic mean diameters in the range 0.4 [6] to 2.6 [2] mm, usually at quite high mass fluxes ($300 < G < 1400$ $\mathrm{kg\,m^{-2}\,s^{-1}}$) and low heat fluxes ($4 < q < 12$ $\mathrm{W\,m^{-2}}$). They have reported that the heat transfer coefficient increases slightly with decreasing diameter and with increasing mass flux. They have found their results to be correlated reasonably well by the approach of Moser et al. [7]. Yang and Webb [2] also noted a dependence of h on the wall heat flux, as $h \propto q^{0.2}$.

Begg et al. [8] studied condensation of water at very low mass fluxes ($G < 5$ $\mathrm{kg\,m^{-2}\,s^{-1}}$) in tubes with diameters from 1.6 to 3.4 mm. Complete condensation occurred in an annular film which fed into a stationary gas–liquid interface that formed across the tubes. The gas was essentially stationary and the results therefore do not shed much light on the flow condensation that occurs at much higher mass fluxes.

Yan and Lin [9] compared the condensation rates of R134a in a pipe with internal diameter 2.0 mm over the ranges $100 < G < 200$ $\mathrm{kg\,m^{-2}\,s^{-1}}$ and $10 < q < 20$ $\mathrm{W\,m^{-2}}$. They found lower heat transfer coefficients at

* Corresponding author. Tel.: +61-2-9351-3435; fax: +61-2-9351-3471.
E-mail address: haynes@chem.eng.usyd.edu.au (B.S. Haynes).

0017-9310/$ - see front matter © 2003 Elsevier Ltd. All rights reserved.
doi:10.1016/S0017-9310(03)00287-4

Nomenclature

The subscripts G and L are used to indicate quantities based on the individual vapour and liquid phases respectively. For annular film calculations, we use a diacritical $'$ to indicate fluxes based on areas relevant to the individual phases.

a	area per length of TEC, m
B	suction parameter ($=q_c/G\lambda$)
c_p	heat capacity, $J\,kg^{-1}\,K^{-1}$
d	internal tube diameter, m
G	axial mass flux, $kg\,m^{-2}\,s^{-1}$
h	heat transfer coefficient, $W\,m^{-2}\,K^{-1}$
H	enthalpy, $J\,kg^{-1}$
k	thermal conductivity, $W\,m^{-1}\,K^{-1}$
I	electrical current, A
$\dot{m}$	mass flow rate, $kg\,s^{-1}$
N	number of junctions in a TEC
Nu	Nusselt number ($=hd/k$)
q	heat flux, $W\,m^{-2}$
Q	heat flow rate, W
Re	Reynolds number ($=Gd/\mu$)
s	Seebeck coefficient, $V\,K^{-1}$
S	slip ratio ($=u'_G/u'_L$)
T	temperature, K
u	velocity, $m\,s^{-1}$
x	quality (mass fraction)

Greek symbols

δ	film thickness, m
ε	volume fraction
λ	latent heat of condensation, $J\,kg^{-1}$
ρ	density, $kg\,m^{-3}$
τ	shear stress, Pa
ϖ	electrical resistivity, $\Omega\,m$

Subscripts

c	condensation (heat flux)
c	cold (temperature)
conv	convection
f	friction
G	gas (vapour) phase
h	hot
i	block number
i	gas–liquid interface
L	liquid phase
PST	Peltier + Seebeck + Thompson effects
sat	saturated gas/liquid
TEC	thermoelectric cooler
th	thermodynamic equilibrium condition
w	wall

higher heat fluxes, especially at high heat fluxes. By comparison with other published data, they concluded that the effect of diameter on heat transfer coefficients is very small.

Wang et al. [10] condensed refrigerant R134a in a 10-port rectangular extrusion with hydraulic mean diameter of the nearly square channels $d_h = 1.46$ mm. Most of their data were in an annular flow regime and showed a strong influence of mass flux ($150 < G < 750$ $kg\,m^{-2}\,s^{-1}$), especially at high quality. Their data were poorly predicted by conventional large-tube correlations—the best predictions were in fact made with the Akers correlation which Webb and coworkers [3–5] had dismissed as erroneous.

These few studies have raised some questions for further research. It is clear that none of the plethora of correlation methods developed for larger-diameter tubes has been validated comprehensively for microtubes. There is also uncertainty about the influence of heat flux and tube diameter on microtube condensation.

Historically, in-tube phase-change heat transfer experiments have been performed in tubes of diameters between 7 and 25 mm [11]. The test passages were usually heated or cooled by a fluid flowing counter-current to the test fluid in an annular enclosure. Because of the small heat loads associated with heat transfer in a single narrow passage, most of the studies mentioned above have been carried out on a number of passages in parallel. A second fluid in cross-flow was generally used as a heat sink, with the amount of heat transferred to the test fluid determined by the enthalpy gain of the second fluid. However, it is extremely difficult to guarantee uniform gas–liquid distribution among multiple channels if the inlet fluid is a partially condensed two-phase mixture. The use of large changes in quality across a test section facilitates determination of the total heat flow but may also obscure trends occurring as the quality changes.

In order to measure heat transfer rates under defined conditions, it is common practice in studies on both small and large diameter tubes, to create a vapour–liquid equilibrium mixture scale by partial condensation in a pre-condenser, and then to introduce that mixture into a test section for measurements at the nominal conditions. Unfortunately, the extent to which the condensation process (e.g. heat flux history) might affect the hydrodynamics of the system cannot be reliably inferred from such measurements.

In this work, we have undertaken a comprehensive study of local condensation rates in fine passages, as a

function of the mass flux, heat flux, vapour quality, pressure, and tube diameter for two fluids. The fluids enter as single-phase, mildly superheated vapour, and the progress of the condensation process in a single tube is tracked.

2. Experimental method

This section describes the basis of the method used to generate uniform wall heat fluxes to study pseudo-local condensation heat transfer in narrow passages. The overall method is similar to that used by us previously to study flow boiling, except that the ohmic heaters are replaced with thermoelectric coolers (TECs). Details of the boiling rig are given in Bao et al. [12,13] and full details of the construction of the condensation rig are given in [14].

2.1. Design of the condensation experiment

The desire to measure heat transfer performance pseudo-locally, and the relatively low rates of heat and fluid flow involved, necessitated a novel apparatus design. In previous work, we have used zone-wise electrical resistance heating to determine pseudo-local heat transfer rates in flow boiling [12,13]. For cooling or condensation studies, we need a quantifiable local heat sink capable of operating at low loads (typically less than 100 W) and relatively high heat fluxes. The TEC can provide this function, with the heat flux being controlled electrically, in much the same way as resistive heating can be controlled. Due to the relative weakness of the thermoelectric effects involved, individual coolers typically transfer less than 100 W (thermal) and are therefore not suitable for large scale industrial cooling applications.

In a TEC, the Peltier, Seebeck and Thompson effects combine to cause a heat flow across a junction when a current is passed through that junction. The heat flow may be expressed as

$$Q_{\mathrm{PST}} = sIT_{\mathrm{c}} \tag{1}$$

There are two unwanted heat flows associated with TEC cooling devices. Joule heating (Q_{J}) arises from electrical resistance to the current, as described by the expression:

$$Q_{\mathrm{J}} = \frac{I^2\varpi}{2a} \tag{2}$$

Thermal conduction between the hot and cold sides (Q_{hc}) also leads to degradation in performance:

$$Q_{\mathrm{hc}} = ka(T_{\mathrm{h}} - T_{\mathrm{c}}) \tag{3}$$

Combining these equations, the net heat transferred to the cold face of a TEC (Q_{TEC}) comprising N junctions is therefore

$$Q_{\mathrm{TEC}} = N\left[sIT_{\mathrm{c}} - \frac{I^2\varpi}{2a} - ka(T_{\mathrm{h}} - T_{\mathrm{c}})\right] \tag{4}$$

The characteristic parameters and material properties are known and provided by the TEC manufacturer. To increase TEC efficiency, the temperature difference across the TEC ($T_{\mathrm{h}} - T_{\mathrm{c}}$) can be minimised by use of a heat sink in the form of a temperature controlled water flow.

Note that the Seebeck effect is reversible so that reversal of the current direction through the TEC allows the device to be operated as a heater. We have in fact used this to study flow boiling [15] but the additional complexity of the device when compared with simple ohmic heating makes the system less controllable and therefore less desirable for establishing particular heating conditions.

2.2. TEC test section design

The design of the apparatus is based on the ohmic heating devices we have described previously [12,13]. The test section consists of 10 essentially contiguous but independently cooled zones, each 30 mm in length and thermally insulated from adjacent zones by 2 mm thick compressed fibre insulation. Each zone comprises a copper block, soldered to the tube wall, to which a TEC (Melcor, model: CP 5-171-31L) is attached, as shown in cross-section in Fig. 1. A non-silicone heat transfer compound is applied to ensure good thermal contact between the TEC faces and the copper blocks. The copper block encasing the tube is isothermal at the cold-face temperature (T_{c}) of the TEC. The hot face of the TEC (at T_{h}) is coupled essentially isothermally, by a second copper block, to the heat sink whose temperature is maintained within ± 0.1 °C by high-velocity water circulation. An air gap and solid plastic spacers serve to isolate the two blocks to ensure that the only significant heat transfer between them is via the TEC faces. Mechanically, the system is held by insulated screws tapping into the plastic spacers. A torque driver was used to tighten the screws to place the TEC under a compressive

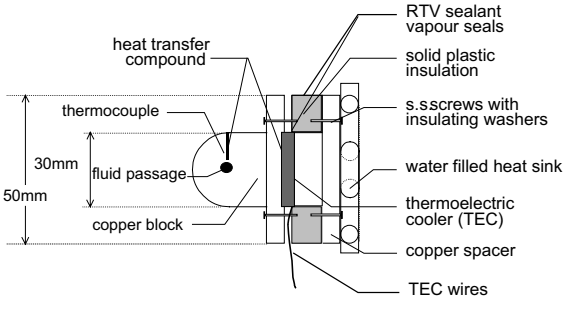

Fig. 1. Schematic of a TEC test section in cross-section.

load of 1500 kPa, in accordance with the manufacturer's instructions.

The copper block attached to the test conduit wall ensures a constant wall temperature over the entire test passage circumference and along the length of the zone. Numerical simulations confirm that this is the case for the range of conditions examined here [14]. In order to measure the block temperature, a type-K thermocouple is inserted into a radial well, diameter 1.6 mm, to within 2 mm of the test passage wall at the midpoint of each block. These holes are filled with a non-silicone heat transfer compound.

The thermal contact resistance between the tube wall and the copper blocks is measured in tests on high-speed water flows to be $\sim 10^{-5}$ $m^2\,K\,W^{-1}$. This resistance is neglected in the present work (in which heat transfer coefficients are $<10^4$ $W\,m^{-2}\,K^{-1}$) and the wall temperature in contact with the fluid is assumed to equal the measured block temperature.

The 10 TEC are connected in parallel to a variable DC power source (Xantrax XFR20-60). Variable resistors (Ohmite 50 W, 6 Ω) are used to adjust the current input to each individual TEC in order to obtain approximately the same heat fluxes to each zone—this was only partly successful as the very low heat transfer coefficients obtained at near complete condensation ($x < 0.2$) required very low wall temperatures, often below the available TEC sink temperature. Under these conditions, the wall heat flux can be significantly lower than at higher qualities.

A continuous length of drawn metal tube runs the entire length of the section. This tube has a 270 mm entrance length to ensure flow is fully developed hydrodynamically before entering the test section, and extends 150 mm past the section outlet to minimise exit effects. Test sections are constructed from straight-rolled tube with inner diameters of 1.95 and 0.92 mm. The 1.95 mm diameter tubes were formed of copper. As straight-rolled copper tubing was unavailable in the smaller size, brass tubing was substituted. The tube diameters were confirmed using single-phase pressure drop measurements, as described in [12].

The thermocouple mountings, entrance, and exit lengths are well insulated with closed cell foam insulation. In addition, the entire test section is insulated from ambient conditions with urethane-based expandable foam insulation.

2.3. Test section calibration and performance

In order for a TEC to be used as a quantifiable heat sink, it must be calibrated to confirm conformity with Eq. (4). The Seebeck coefficient and electrical resistivity of the semiconductor material from which a TEC is made are sensitive to the physical pressure applied. Therefore, it is critical that each TEC be tested and subsequently installed in a manner that allows a consistent and even force to hold it in place.

Testing of individual TECs was carried out in a specially constructed system. The TEC was sandwiched between two copper blocks whose temperatures were controlled by circulating water streams. The same non-silicone heat transfer compound and compression loading of the TEC as employed in the test section was employed. The heat transfer rate across the TEC was calculated from the temperature changes in the water streams to the copper blocks and compared with the values predicted from Eq. (4). The heat balances were conducted using cooling loads between 7 and 20 W and temperatures in the range 15–75 °C and were generally found to be accurate to within 5%—outside this limit, the TEC was rejected. Of the 13 TECs tested for use in the 1.95 mm passage diameter apparatus, two were rejected.

Inlet and outlet fluid temperatures are measured with thermocouples placed in the flow upstream and downstream of the test section. The thermocouple voltage for each block is measured differentially with respect to the fluid inlet thermocouple voltage. The fluid inlet thermocouple readings are compensated for ambient temperature using a four-wire resistance thermometry device mounted isothermally with the thermocouple junction box. The accuracy of each thermocouple was verified using an ice water bath, boiling water at atmospheric pressure, and a constant temperature water bath, whose temperature was measured with a mercury-in-glass thermometer calibrated to ±0.05 K. Wall temperatures are accurate to better than ±0.08 K using this differential technique.

As described in our previous work on boiling [12,13,15], a detailed heat balance is carried out on each block in order to determine the zone-averaged wall heat flux. Corrections are made to the TEC heat flow to allow for interblock heat transfer and for heat flow from the surroundings. The conductance coefficients for these heat flows are determined in a series of calibration experiments under no-flow conditions. Under test conditions with fluid flow, the heat in-leakage from the surroundings is always less than 10% of the TEC load and is quantified within 1.5% of the TEC load. Interzonal heat transfer is less than 15% of the TEC load and is known to within 2% of the TEC load. With the uncertainty in the TEC calibration itself being <5%, the magnitude of the heat transfer rate to the fluid in a zone is therefore known to better than 10% uncertainty.

The fluid enthalpy at zone i is estimated from the cumulative heat flow from entry to the test section to the midpoint of the zone

$$H_i = H_{i-1} + \frac{Q_{i-1} + Q_i}{2\dot{m}} \tag{5}$$

Overall heat balances under single-phase liquid flow conditions, or with total condensation of vapour, are

generally within 10% and always within 20% of the sum of the 10 TEC loads. The local fluid properties and temperature at zone i are calculated as a function of the local fluid enthalpy (Eq. (5)) and the estimated pressure at the location, using the NIST Refprop 6.01 database [16]. As described below in Section 3.1, measured pressure drops across the whole test section are well correlated (±20%) by Lockhart–Martinelli correlation and this correlation was therefore used to calculate the pressure drops from entry to the zone in question.

Apparent local heat transfer coefficients are then calculated as

$$h_i = \frac{q_i}{T_{\text{sat}}|_i - T_{\text{wall}}|_i} \tag{6}$$

The application of Eq. (6) to condensation from superheated vapour, as occurs in the first block in all tests, and in later blocks in some cases at relatively low heat flux, is discussed in more detail in the discussion section of this paper.

Measurements of local single-phase heat transfer coefficients in thermally developing laminar flow agree with theoretical predictions within 20% and the uncertainty in the condensation heat transfer coefficients is estimated also to be of this order (see Table 1).

2.4. The refrigerant loop

Fig. 2 shows the overall circulation loop for the test fluid. Subcooled liquid is pumped by a variable-speed gear pump, that is in turn controlled via a coriolis-effect mass flow meter/controller with three term PID (ABB K-Flow model K-2, calibrated accuracy better than ±2%). System pressure is controlled (±1%) independently of the bulk fluid temperature via a controlled electrically heated reservoir. In this arrangement, the saturation pressure of the fluid within the reservoir determines system pressure. Power to the reservoir heater is controlled by a three term PID controller (Gefran 500) connected to an inline pressure transducer (TransInstruments 2000).

The inlet fluid pressure is measured by an absolute pressure transducer (Yokogawa model EJA310A) while a differential pressure transducer (Yokogawa model EJA110A) measures the pressure drop across the test section. The calibration of these transducers is better than ±0.2%, as periodically verified against a NIST-traceable pressure calibrator (Druck DPI-602).

A water-heated pre-boiler sets the fluid temperature at the entrance to the test section. During condensation experiments, the test fluid is completely vapourised in the pre-boiler, typically entering the test section with 10–15 K of superheat. After exiting the test section, any remaining vapour is condensed and subcooled via a chilling circuit before being returned via the pump and flow meter to the pre-boiler.

Table 1
The range of experimental parameters and relevant uncertainties studied for flow condensation heat transfer

Parameter	Range	Uncertainty
Fluid	HCFC-123, R11	
Passage diameter, d	0.92, 1.95 mm	±1%
System pressure, p	120–410 kPa	±0.2% at entry
Saturation temperature, T_{sat}	20–72 °C	<1 °C
Mass flux, G	70–600 $\text{kg m}^{-2}\,\text{s}^{-1}$	±5%
Heat flux, q	15–110 kW m^{-2}	±10%
Thermodynamic vapour quality, x_{th}	<0–1.05	±0.05
Driving force, ΔT_{sat}	4–40 K	±0.3 °C
Pressure drop, $\Delta p_{\text{overall}}$	~0–100 kPa	±2 kPa
Liquid Reynolds number, Re_{L}	0–2100	
Inlet vapour Reynolds number, Re_{G}	16,000–100,000	
Inlet suction parameter, $B = q/G\lambda$	0.0001–0.008	
Heat transfer coefficient, h	0.5–10 $\text{kW m}^{-2}\,\text{K}^{-1}$	20%

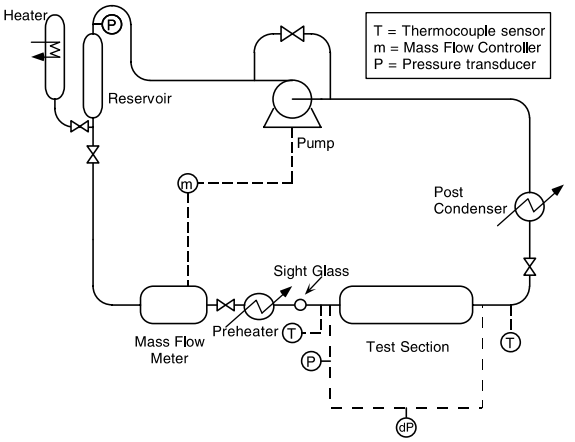

Fig. 2. Schematic of the refrigerant loop.

Exhaustive outgassing of the test loop and of the test fluid is undertaken prior to any experiments. After the system is evacuated ($p < 1$ Pa), a volume of ~20 ml of liquid test fluid is injected into the system and allowed to evaporate through the loop to scavenge any remaining contaminants. The system is evacuated again and charged with the test fluid. By heating the reservoir, the system is pressurised to about 6 bar (which is greater than the pressure at which tests are carried out). The test fluid is then circulated and vapour head spaces are bled.

3. Results

Results have been obtained over a wide range of conditions, for two refrigerant fluids, R11 and HCFC-123, as summarised in Table 1.

3.1. Pressure drop

The measured pressure drop, Δp_{obs}, derives not only from the frictional pressure drops in the condensation test section, but also from an accelerational component and from friction components in the entry and exit sections. Predicted pressure drops are thus calculated as

$$\Delta p_{overall} = \Delta p_f|_{entry} + \Delta p_a|_{test\ section} + \sum_{i=1}^{10} \Delta p_f|_i + \Delta p_f|_{exit} \quad (7)$$

where the entry pressure change is calculated for single-phase turbulent gas flow and the accelerational pressure change over the test section is that for separated flow [17]. The two-phase frictional pressure changes incurred through the 10 zones of the test section and in the exit length are calculated from an appropriate two-phase method.

Since the fluid invariably enters as a superheated vapour, the frictional losses in the long entry section are often dominant, amounting to 3–5 velocity heads (based on the incoming vapour, $G^2/2\rho_V$). The accelerational term corresponds typically to a pressure rise (negative drop) in the range of 1–2 gas velocity heads. The test section itself generally contributes only a few velocity heads, so the present arrangement does not provide a good basis for studying pressure drops in condensing flows. However, it remains important to obtain a reasonable estimate of the pressure profile in the test section as this influences the properties and saturation temperature of the fluid in the zones.

Fig. 3 shows a comparison of the overall measured pressure drops for the experiments with those predicted when the Lockhart–Martinelli correlation [18] is employed for the two-phase frictional pressure losses. Also shown are the predictions derived using the annular shear stress model described in Section 4. Overall, the Lockhart–Martinelli correlation reproduces the observations reasonable well and this equation is therefore used to estimate the zonal pressure drops. These are scaled so that the overall calculated pressure drop equals the measured value, so as not to induce a discontinuity in the calculated saturated fluid properties. Note however, that so long as the entrance effects are substantially accounted for, the calculation of local heat transfer coefficients is not particularly sensitive to the pressure interpolation procedure. Thus, the use of the scaled shear stress method or even of the unscaled Lockhart–Martinelli method produces essentially identical heat transfer coefficients in the analysis.

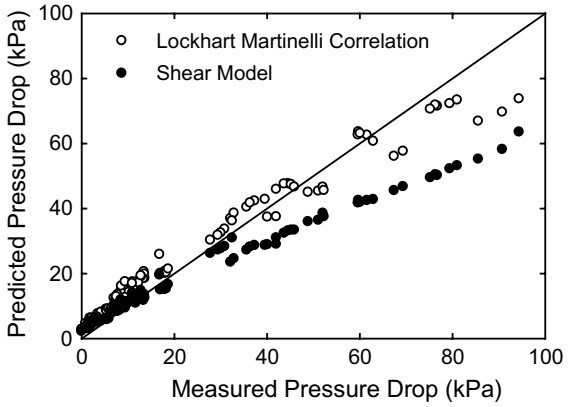

Fig. 3. Comparison of predicted and experimental overall pressure drops. The two-phase predictions are based on the standard Lockhart–Martinelli correlation (○) or on the annular shear model described in the text (●).

3.2. Condensation heat transfer

Fig. 4 shows typical observations of test section wall temperature, T_w, equilibrium fluid temperature, T_f, wall heat flux, q, thermodynamic liquid fraction, $1 - x_{th}$, and apparent heat transfer coefficient for refrigerant HCFC-

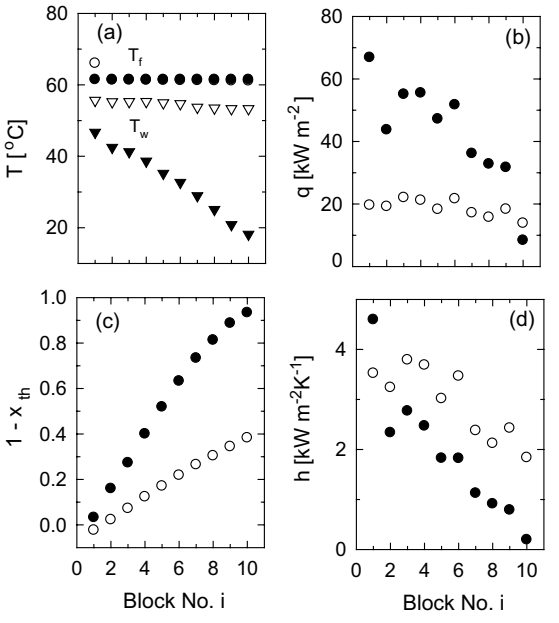

Fig. 4. Typical results for condensation of HCFC-123 ($G = 170$ kg m^{-2} s^{-1}) condensing in a 1.95 mm diameter tube. Results are shown for heat flux 20 kW m^{-2} (○) and for an average heat flux of ~45 kW m^{-2} (●).

123 ($G = 170\ \mathrm{kg\,m^{-2}\,s^{-1}}$) condensing in a 1.95 mm diameter tube. Results are shown for a relatively low value of heat flux (20 $\mathrm{kW\,m^{-2}}$) that leads only to partial condensation, as well as for a higher (average ~45 $\mathrm{kW\,m^{-2}}$) heat flux that leads to complete condensation at the exit of the test section. At $q = 20\ \mathrm{kW\,m^{-2}}$, the changes in the system behaviour from the first to the last block were small enough to enable the wall heat flux to be held constant. On the other hand, at the higher heat flux, the decreasing heat transfer coefficient encountered especially at higher degrees of condensation ultimately demanded a very low wall temperature which in turn affected the TEC performance and precluded the establishment of a constant wall heat flux through all the sections.

Comparison of data over many runs suggests that the measured local heat transfer coefficient is determined essentially only by the local block conditions. Therefore, in all the data presentations that follow, the data for nominal condensation conditions are extracted from the total pool of results with acceptance bandwidths of ±10% around the nominated values for G, q and p. Thus, a presentation of results with nominal heat flux of 60 $\mathrm{kW\,m^{-2}}$ will include results in the range $54 < q < 66\ \mathrm{kW\,m^{-2}}$. The acceptance bandwidth for results at a nominal value of x is set a constant value of ±0.05 in order to provide better discrimination at high values of x.

3.2.1. The effect of mass flux and vapour quality

The observed heat transfer coefficients generally increase with increasing mass flux. The points in Fig. 5 show HCFC-123 results for various total mass fluxes with $q = 60\ \mathrm{kW\,m^{-2}}$ at a pressure of 290 kPa in a tube of diameter 1.95 mm. The influence of mass flux is relatively most pronounced at lower values of G and at higher values of the liquid mass fraction ($1 - x_{\mathrm{th}}$).

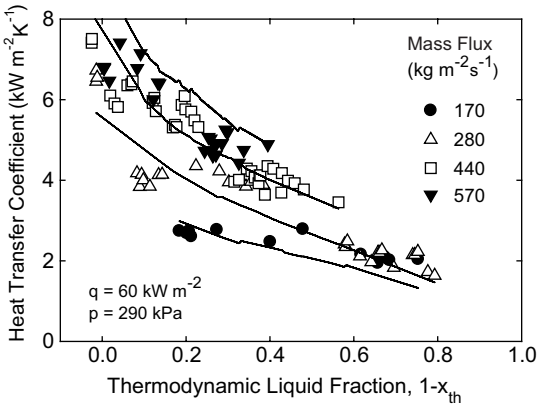

Fig. 5. Effect of mass flux on the heat transfer coefficient for condensation of HCFC-123 in a 1.95 mm tube, with wall heat flux 60 $\mathrm{kW\,m^{-2}}$ at 290 kPa. Points show experimental results while lines show predictions of the annular shear model described in the text.

3.2.2. The effect of heat flux

The condensation heat flux has a significant influence on heat transfer coefficients, particularly at lower values of the liquid mass fraction. Fig. 6 shows results for condensation of HCFC-123 at 290 kPa in a 1.95 mm diameter tube, for a constant overall mass flux of $G = 440\ \mathrm{kg\,m^{-2}\,s^{-1}}$. While the points at the lowest values of heat flux could only be obtained at low liquid fractions, it is quite clear that the influence of condensation mass flux on the heat transfer coefficient for the process diminishes as the liquid fraction increases.

3.2.3. The effect of system pressure

Increasing system pressure at constant wall heat flux and constant total mass flux leads to a decrease in the local heat transfer coefficients, especially at and just beyond the onset of condensation, $x_{\mathrm{th}} \sim 0$, as can be seen in Fig. 7.

3.2.4. Effect of passage diameter

While most of the runs (>2000 points) in this study were carried out with a passage diameter of 1.95 mm, a few runs (55 points) were conducted with a passage diameter of 0.92 mm. These had to be at somewhat higher mass fluxes (350–660 $\mathrm{kg\,m^{-2}\,s^{-1}}$) and heat fluxes (50–200 $\mathrm{kW\,m^{-2}}$) than used in the larger tube in order to operate in regions where the absolute heat and mass flows were measurable and controllable. Fig. 8 shows a comparison of results obtained for HCFC-123 in the two tubes under similar conditions of pressure and heat and mass flux. The magnitudes of the heat transfer coefficients are obviously very close throughout the course of the condensation process.

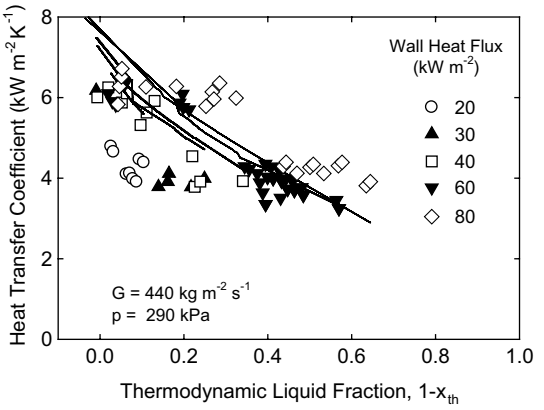

Fig. 6. Effect of wall heat flux on the heat transfer coefficient for condensation of HCFC-123 in a 1.95 mm tube, for total mass flux 440 $\mathrm{kg\,m^{-2}\,s^{-1}}$ at 290 kPa. Points show experimental results while lines show predictions of the annular shear model described in the text. The uppermost line corresponds to the highest heat flux with lower lines corresponding in order to lower heat flux.

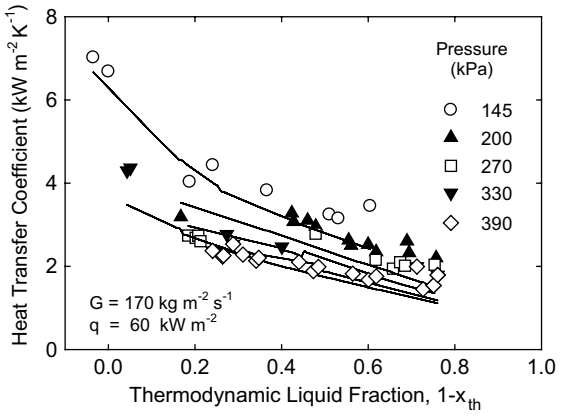

Fig. 7. Effect of system pressure on the heat transfer coefficient for condensation of HCFC-123 in a 1.95 mm tube, for total mass flux 170 kg m^{-2} s^{-1} with wall heat flux 60 kW m^{-2}. Points show experimental results while lines show predictions of the annular shear model described in the text. The uppermost line corresponds to the lowest pressure with lower lines corresponding in order to higher pressures.

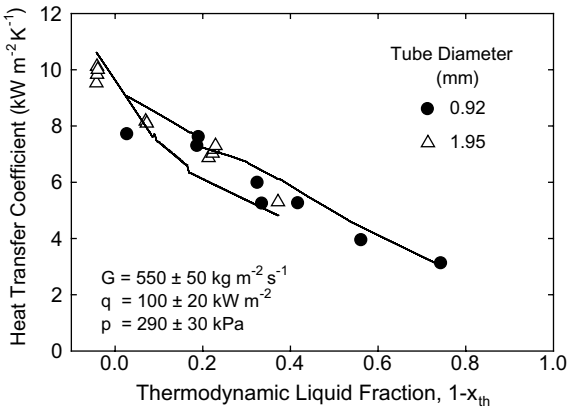

Fig. 8. Effect of passage diameter on heat transfer coefficient for condensation of HCFC-123 for total mass flux 550 kg m^{-2} s^{-1} with wall heat flux 100 kW m^{-2}, at pressure 290 kPa. Points show experimental results while lines show predictions of the annular shear model described in the text. The upper and lower lines correspond to $d = 0.92$ mm and $d = 1.95$ mm, respectively.

3.2.5. Results for R11

A large set of data (800 points) was obtained for flow condensation of R11 in the 1.95 mm tube [14] but is not presented here in detail as the results are qualitatively very similar to those obtained with HCFC-123.

3.2.6. Comparison with published correlations

The heat transfer coefficients obtained in this work have been compared with the predictions of a large number of correlations, including Akers et al. [19], Boyko and Kruzhilin [20], Azer et al. [21], Moser et al. [7], Traviss et al. [22], Dobson and Chato [23], and Shah [11]. Here in Fig. 9 we show the summary of the comparison of the predictions of the Shah method [11] with all of the HCFC data ($Re_{LO} > 350$). The Shah correlation clearly overpredicts most of the data throughout the course of the condensation; in addition, there is great variability in the quality of the prediction. The same level of scatter and overprediction is also found with the R11 comparison. Yang and Webb [2] also found the Shah correlation to overpredict their data which was obtained with R12 in tubes with a hydraulic mean diameter of 2.6 mm.

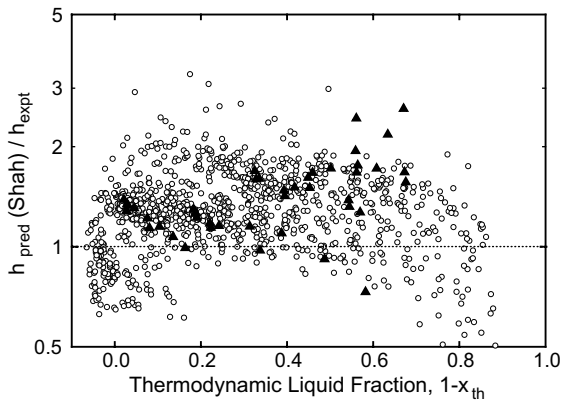

Fig. 9. Comparison of the predictions of the Shah correlation [11] with experimental heat transfer coefficients for all HCFC-123 data. Tube diameters 1.95 mm (○) and 0.92 mm (▲).

The other correlations tested generally provide similar or worse representation of the experimental data than shown in Fig. 9. Details of these results are presented elsewhere [14].

4. Discussion

It is well accepted that condensation heat transfer rates are intimately connected to the hydrodynamics of the two-phase vapour/liquid flows under the particular conditions. Modern approaches to modelling or correlating convective condensation rates attempt to take this into account explicitly, with the basic distinction in horizontal channels being between gravity-dominated and shear-dominated flows. Surface tension forces may also be an issue in some systems.

Many studies of non-condensing gas–liquid flows in fine passages have pointed to the predominance of annular liquid-film flows over broad regions of the flow map [12,24]. On the basis of the superficial gas and liquid velocities obtaining in the present measurements, all of the data points with vapour quality $x > 0.20$ are

therefore expected to be in an annular flow regime, frequently perhaps with a wavy gas–liquid interface. One would expect there to be an even greater tendency for annular flows to develop during condensation which will always give rise to some film of liquid around the circumference of the tube.

The limiting case of shear-dominated annular flow provides the basis for a predictive model development, as has been described many times in the literature previously [17,21,22,25–30]. In terms of the usual variables employed in turbulent film theory, the heat transfer coefficient for the liquid film may be expressed as

$$h = \frac{c_{pL}\sqrt{\rho_L \tau_w}}{T_\delta^+} \tag{8}$$

Here T_δ^+ is the dimensionless temperature defined at the vapour–liquid interface of the film. This quantity is easily obtained from a simple turbulent boundary-layer analysis using the universal velocity profile for turbulent wall flows and is represented by

$$\begin{aligned} T_\delta^+ &= \delta^+ Pr_L \quad \text{for } \delta^+ < 5 \\ &= 5\left\{ Pr_L + \ln\left[1 + Pr_L\left(\frac{\delta^+}{5} - 1\right)\right]\right\} \\ &\quad \text{for } 5 \leqslant \delta^+ \leqslant 30 \\ &= 5\left\{ Pr_L + \ln[1 + 5Pr_L] + \frac{1}{2}\ln\left(\frac{\delta^+}{30}\right)\right\} \\ &\quad \text{for } \delta^+ > 30 \end{aligned} \tag{9}$$

where $\delta^+ = (\delta\sqrt{\rho_L \tau_w})/\mu_L$.

In order to evaluate the dimensionless film thickness, measures of the actual film thickness δ and of the wall shear stress τ_w are required. For the film thickness, some authors [28] employ an empirical correlation for liquid (or vapour) volume fraction. More self-consistently, however, the same film analysis as employed for the heat transfer calculations may be used to relate the film mass flow to the height of the film. We employ this latter approach, using the result of Henstock and Hanratty [31]:

$$\delta^+ = \left\{ \left(0.7071\, Re_L^{0.50}\right)^{2.5} + \left(0.0379\, Re_L^{0.90}\right)^{2.5} \right\}^{0.4} \tag{10}$$

In Eq. (10), the left hand term in the brackets corresponds to the result for a film that is thinner than the laminar sublayer thickness calculated from the universal velocity profile (i.e. to $\delta^+ < 5$, and thus to $Re_L < 50$). The right hand term represents the limit of a film that is thicker than the predicted limit of the transition layer (i.e. to $\delta^+ > 30$, and thus to $Re_L \gtrsim 1500$). Note that shear-driven flows become turbulent at much lower values of Re_L than the value of $Re_L \sim 1600$ corresponding to the laminar–turbulent transition in vertical gravity-driven film flow. However the above equations cannot be taken to suggest that shear-driven flows with $Re_L > 50$ are necessarily turbulent.

The usual force balance on the liquid film relates the axial frictional pressure gradient to τ_w

$$\frac{-\mathrm{d}p_f}{\mathrm{d}z} = \frac{4\tau_w}{d} \tag{11}$$

and one can therefore use a pressure-drop correlation to estimate τ_w, which is the usual approach [17,27]. However, a correlation developed for non-condensing flows may not be valid for condensing flows, in particular because there is additional momentum transfer from the gas to the liquid associated with the process of condensation.

In general, τ_w can be related to the mean vapour–liquid interfacial shear stress, τ_i, through an axial momentum balance on the liquid film:

$$(d - 2\delta)\tau_i = \mathrm{d}\tau_w \tag{12}$$

In two-phase annular flows, the fast-moving gas core exerts a frictional drag on the surface of the liquid. This is usually described in terms of a conventional frictional factor for duct flow, where the velocity is based on the mass flow of gas and the open flow area. Much attention has been given to the apparent surface roughness effect of waves and other disturbances on the liquid surface and correlations have been developed for this effect. However, it is not clear to what extent this approach is valid for condensing flows which correspond closely to flows with "wall suction" in single-phase situations. It is well known that wall suction (the transfer of mass from the gas core through the duct boundary) has a marked laminarizing effect on the boundary layer, thus reducing the wall friction.

In addition to providing a wall suction effect on the vapour flow, the condensation of vapour into the liquid directly provides an additional source of momentum transfer to the liquid. If the gas core friction is unaffected by wall suction, then a simple additive model provides the total rate of momentum transfer (shear force) from the gas to the liquid:

$$\begin{aligned} \tau_i &= \frac{\rho_G u_G'^2}{2} f_G' + \left(\frac{q_{i,c}}{\lambda}\right)(u_G' - u_L') \\ &= \frac{\rho_G u_G'^2}{2}\left(f_G' + 2\left(\frac{q_{i,c}}{\rho_G u_G' \lambda}\right)\left(1 - \frac{1}{S}\right)\right) \\ &= \frac{\rho_G u_G'^2}{2} f_{eff}' \quad \text{where } f_{eff}' \approx \left(f_G' + 2B_G'\right) \quad \text{when } S \gg 1 \end{aligned} \tag{13}$$

where the dimensionless group $B_G' = q_{i,c}/G_G'\lambda$ is closely related to the boiling number familiar from studies of flow boiling and evaporation. It is equivalent to the suction parameter in wall flows with suction, being the ratio of the wall suction and axial mass fluxes. In this term, we see a potential source of the influence of the

condensation rate on the heat transfer coefficient observed in the experiments.

However, as observed above, the presence of wall suction actually modifies the frictional drag term. Hewitt et al. [27, p. 603] present an Ackermann-type analysis of the overall effect, leading to the result for condensation that may be written as

$$f'_{\text{eff}} = \frac{2B'_{\text{G}}}{1 - \exp\left(\frac{-2B'_{\text{G}}}{f'_{\text{G}}}\right)} \tag{14}$$

Kinney and Sparrow [32] carried out detailed numerical calculations of single-phase flows with wall suction and obtained results that were well correlated as

$$f'_{\text{eff}} = f'_{\text{G}} + 1.4B'_{\text{G}}, \quad \text{for } B'_{\text{G}} < 0.02 \quad \text{and} \quad 10,000 < Re'_{\text{G}} < 150,000 \tag{15}$$

A similar calculation was reported by Groenewald and Kröger [33] who provided a more complex empirical fit (over a limited range) to their results in terms of B'_{G} and Re'_{G}. Sofialidis and Prinos [34] also carried out a similar series of calculations, employing a variety of modern turbulence transport models and obtained entirely similar results.

Fig. 10 summarises the results reported for the interfacial drag in smooth-walled systems with wall suction. The influence of wall suction becomes discernible when $B'_{\text{G}} > 10^{-4}$ but is not a significant effect until $B'_{\text{G}} > 10^{-3}$, and is dominant at $B'_{\text{G}} > 10^{-2}$. The Ackermann description and the computational results provide surprisingly similar results for f'_{eff} throughout the range of interest, while the simple additive model is significantly in error. However, in the limit $B'_{\text{G}} \gg f'_{\text{G}}$, the result that $f'_{\text{eff}} = 2B'_{\text{G}}$ is obtained both with the additive model and with the Ackermann analysis but the computational

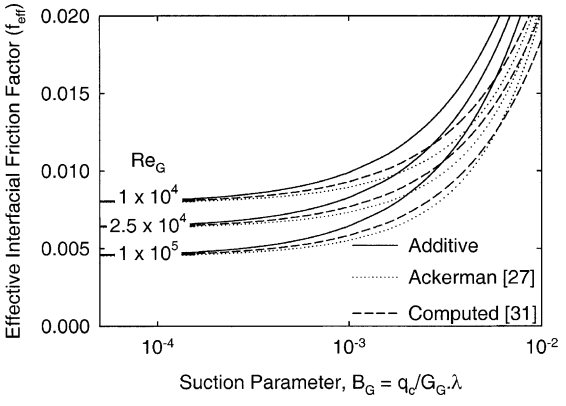

Fig. 10. Effect of wall suction on wall friction factor determined by simple addition (Eq. (13), solid line), by an Ackermann analysis (Eq. (14) [27], dotted line) and as computed via a turbulent transport model (Eq. (15) [32], dashed line).

results [32,34] suggest a somewhat lower dependence of f'_{eff} on B'_{G} as the limit is approached ($B'_{\text{G}} > 10^{-2}$). The strong suction limit assumed by Shekriladze and Gomelauri [35] to be the usual case in condensation is thus an unlikely and probably invalid extreme in most situations.

In this work therefore, we have employed the simple result of Kinney and Sparrow [32], Eq. (15), to describe the combined effects of turbulent friction and condensation on the gas–liquid interfacial drag. The mean gas core velocity is related to the volume fraction of gas

$$u'_{\text{G}} = \frac{xG_{\text{GO}}}{\rho_{\text{G}}\varepsilon_{\text{G}}} \quad \text{where } \varepsilon_{\text{G}} = \left(1 - \frac{2\delta}{d}\right)^2 \tag{16}$$

With a suitable estimate of the core-annular interfacial friction factor in the absence of mass transfer effects, f'_{G}, we may therefore solve Eqs. (11), (12) and (16) to obtain δ, τ_{w}, $\mathrm{d}p_{\text{f}}/\mathrm{d}z$, and h if the local wall heat flux and local quality are known. The experiments return pseudo-local values of the heat flux but the quality calculated from the cumulative heat transfer from entry of the superheated vapour depends somewhat on the assumptions made about the relative extents of sensible (desuperheating) and latent (condensing) heat transfer.

The issue of convective condensation from superheated vapour has been considered recently by Webb [36] and Mills [37]. Here we follow Mills' recommendation that the Ackermann analysis be used to estimate the convective component of the heat transfer from the superheated vapour in the presence of condensation. This gives the effective convective Stanton number as

$$St'_{\text{eff}} = \frac{B'_{\text{G}}}{1 - \exp\left(\frac{-B'_{\text{G}}}{St'_{\text{G}}}\right)} \tag{17}$$

which again is in good agreement with the predictions of detailed turbulence models [32,34]. Therefore, the sensible heat flux and thus the condensation heat flux may be estimated:

$$q_{i,\text{conv}} = h'_{\text{conv,eff}}(T_{\text{G}} - T_{\text{sat}}) \qquad q_{i,\text{c}} = q_{i,\text{tot}} - q_{i,\text{conv}}, \quad \text{where } q_{i,\text{tot}}(d - 2\delta) = q_{\text{w}}d \tag{18}$$

The liquid film flow rate is easily estimated then from the integrated condensation heat flux. Under the conditions studied in this work, for which the initial superheat is only about 10 °C, the condensation flux is always much larger than the convective flux. This analysis therefore leads to estimates of the local quality that are substantially different from the thermodynamic quality, especially in the desuperheating and early saturated condensation phases, as shown for a typical case in the bottom panel of Fig. 11. The middle panel of Fig. 11 shows the corresponding gas temperatures which are predicted to approach the saturation temperature only

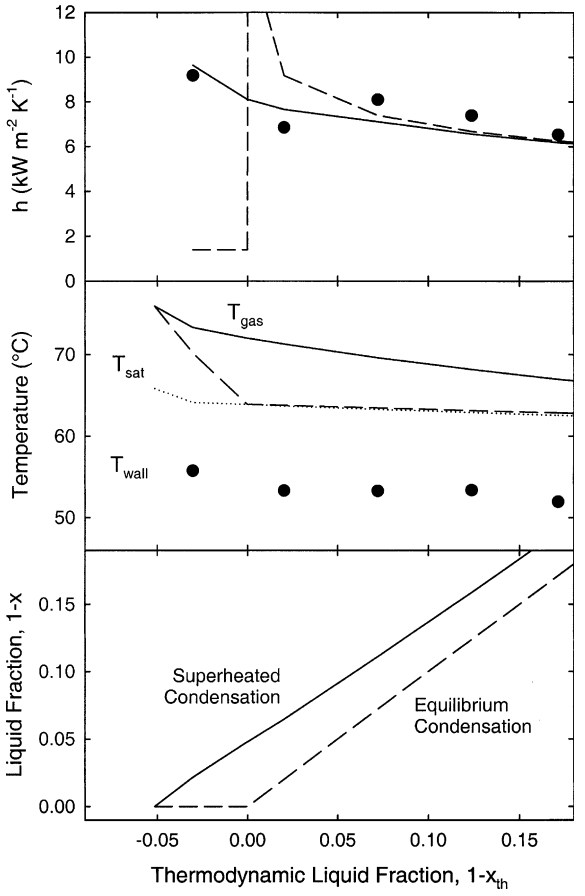

Fig. 11. Illustration of the differences between assuming equilibrium and superheated vapour condensation. Points show experimental data for the first five blocks while lines (solid for superheated condensation; dashed for equilibrium condensation) show calculated quantities. For superheated condensation, there is liquid formation under nominally superheated conditions (bottom panel); slow approach of core gas temperature to the saturation temperature (middle panel); and smooth behaviour of the heat transfer coefficient throughout (top panel).

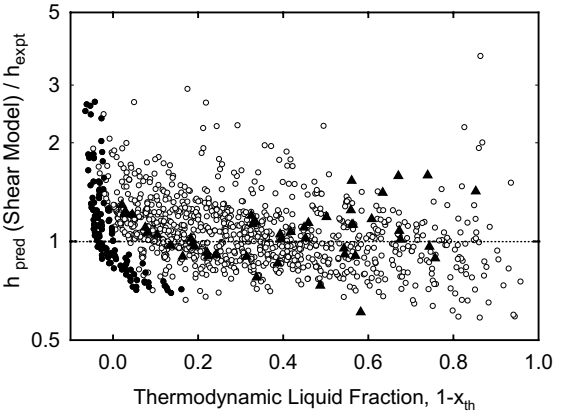

Fig. 12. Comparison of the predictions of the shear model with experimental heat transfer coefficients for all HCFC-123 data. Tube diameters 1.95 mm (first block ●, blocks 2–10 ○) and 0.92 mm (▲).

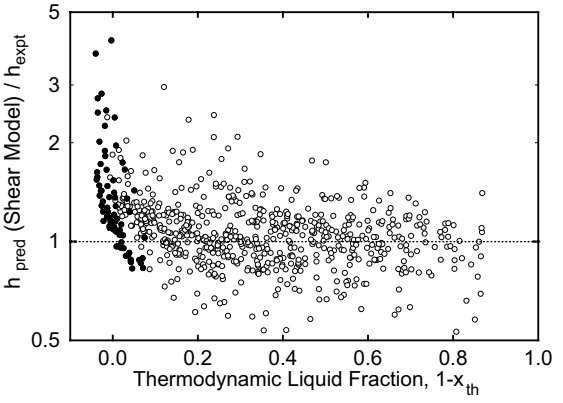

Fig. 13. Comparison of the predictions of the shear model with experimental heat transfer coefficients for all R11 data. Tube diameter 1.95 mm (first block ●, blocks 2–10 ○).

well into the nominal saturation region. The predicted heat transfer coefficients are shown in the top panel of Fig. 11—the assumption of superheated convection gives a very different behaviour from dry-walled gas convection in the region $1 - x_{th} \lessapprox 0$ but beyond that, as the liquid film builds up and becomes turbulent, the predictions converge.

In the absence of validated expressions for the interfacial friction in fine passages, and to be fully consistent with the implied smooth core-annular interface in the one-dimensional model formulations above, we take the friction factor for the gas core flow to be that for smooth passages, $f_i = 0.079 Re^{-1/4}$. Summaries of the agreement between model prediction and experiment, as $h_{\text{prediction}}/h_{\text{experimental}}$ are presented in Figs. 12 and 13 for HCFC-123 (diameters of 0.92 and 1.95 mm) and R11 ($d = 1.95$ mm), respectively. In both cases, the mean value of $\ln(h_{\text{prediction}}/h_{\text{experimental}})$ is 1.05 with a standard deviation of 0.25. Clearly, the average prediction is substantially closer to the experimental value than was found for the Shah correlation but the scatter remains similar and somewhat higher than the estimated uncertainty (10–20%) of the experimental results. Closer examination reveals the prediction to be worse at high values of the liquid fraction and also at very low values of this quantity. In the former case, it is possible that the flow conditions are no longer annular, thus invalidating the basic assumptions of the model; in addition the actual values of the heat transfer coefficients are lowest

here so absolute magnitude of the errors may actually be quite small in this region.

In the region of low liquid fraction, the deterioration in the prediction is apparently not due to any failure to account correctly for the occurrence of condensation while the fluid remains nominally superheated. Fig. 11 (top panel) confirms that the model predictions and the experimental data agree very closely in this region. However, the film model itself cannot really capture the details of the onset the condensation and in a formal sense is indeterminate at this point. Narain et al. [39] has considered the asymptotic forms of shear models that are required of such a model to make the equations solvable at this point. However, it suffices here to point out that our blockwise integration of the local heat (and condensation) fluxes will tend to underestimate the impact of the very high rates of condensation occurring as the first liquid is laid down, which invariably occurs in the first block. This leads to the estimate of the liquid fraction for the block centre being less than is actually the case at that location and therefore to an overprediction of the heat transfer coefficient there, relative to the experimental (blockwise) averaging. The magnitude of this effect is variable, depending on how much the condensation rate changes through the block, but beyond the first block, the effect is negligible. The data points from the first block have therefore been shown as filled circles in Figs. 12 and 13. For these points, the average overprediction is ~25%.

The ability of the annular film model to describe the specific trends observed in the experiments is shown by the solid lines in Figs. 3, 5–8 and 11. The direct effects of mass flux (Fig. 5), system pressure (Fig. 7), and system diameter (Fig. 8) are well represented by the model, within the accuracy of the experimental results. The influence of mass flux and system pressure arise principally in the interfacial frictional shear force which varies as G^2/ρ_G. Secondary effects of mass flux come through the suction parameter ($q/G\lambda$); pressure also has some secondary effects through changes in the saturation temperature of the fluid and attendant changes in properties, especially the liquid viscosity.

The weak effect of tube diameter found here is in accord with results from other studies in fine passages. Thus, Yan and Lin [9] found that, at the same operating conditions, heat transfer coefficients for condensation of R134a averaged over the entire quality range were 10% higher in 2 mm diameter tubes than in 8 mm diameter tubes. Recently, Webb and Ermis [6] reported results for R134a condensation in a series of non-circular extruded aluminium tubes, with $0.44 < d_h < 1.56$ mm. Overall they found higher heat transfer coefficients in the smaller tubes but the comparison were obscured somewhat by lack of dimensional similarity and the presence of microfins in some sections. The weak effect of diameter on the heat transfer coefficient arises through a number of effects, including the fact that, under most conditions, the liquid film is turbulent ($\delta^+ > 5$) which greatly reduces the impact of diameter-scaling on the film heat transfer.

One influence that is relatively poorly captured by the model is that of the wall heat flux. As can be seen in Fig. 6, the model predicts only about 25% of the effect of variations in this parameter in the region of low liquid fraction. This deficiency may also be seen in the comparison of model and experiment for the first heat transfer block (filled circles) in Figs. 12 and 13—the ratio of prediction to experiment decreases systematically in this region as the extent of condensation (essentially, $q/G\lambda$) increases. At higher liquid fractions in Fig. 6, the effect of heat flux decreases and the agreement between prediction and experiment is about as good as can be expected, given the noise in the data.

Dependence of condensation heat transfer coefficients on heat flux has been reported previously. Thus, in experiments carried out in larger diameter tubes with R12 [19] and steam, R11, and R113 [38] showed heat transfer coefficients increasing with increasing heat flux. Kaushik and Azer [38] correlated the effect as $q^{0.2}$, a result which was also found for condensation of R12 in nearly square ducts with $d_h = 2.6$ mm [2]. In contrast to these reports, Yan and Lin [9] concluded that condensation heat transfer coefficients were higher at a heat flux of 10 kW m^{-2} than at 20 kW m^{-2}, for condensation of R134a in circular passages of 2 mm diameter.

The greatest influence of the wall heat flux on the model predictions comes through the influence of mass transfer on the interfacial shear force (Eq. (14) or (15)); there is also a weak effect arising from changes in the mean liquid film viscosity as the wall temperature adjusts to create the imposed heat flux. In terms of the parameter $B_G = q/G_G\lambda$, the effect of mass transfer in the model is weakest at the entry to the test section (highest G_G) and increases as condensation continues. At the same time, as the film accumulates and becomes turbulent, and interfacial shear force declines, the heat transfer prediction becomes less sensitive to the details of the interfacial shear model with the result that the overall impact of mass transfer remains more or less constant through the condensation process.

This analysis suggests that there is a deficiency in the attempt to model the experimental results, especially in the early condensation region. We do not believe that the problem lies in the experimental data as there is no reason to suspect that there are particular problems with the first few blocks, the particular issues associated with the first block having been discussed above. Rather, we suggest that the influence of mass transfer on the incipient film flow is not properly described by the fully developed, turbulent film model we have employed.

Further evidence that the simple smooth film model is inadequate in describing the full extent of the inter-

facial shear lies in the comparison of measured and predicted pressure drops in Fig. 4. The smooth model (with mass transfer effects) accounts only for about 70% of the measured pressure drop or for about 60% of the test-section pressure drop, once entrance effects and acceleration terms are accounted for. The Lockhart–Martinelli correlation provides a good representation overall (albeit with more scatter). However, if the core-annular friction factor in Eq. (14) is taken from the Lockhart–Martinelli correlation, the increased shear force causes the film to become thinner, and the predicted heat transfer coefficients increase by about 50% on average. At the same time, the relative contribution of mass transfer to the effective friction factor (Eq. (14)) decreases and the model predicts essentially no influence of the condensation rate. Groenewald and Kröger [33] have further suggested that the suppression of turbulent shear by the mass transfer effect should not apply to any "non-smooth" contribution of the flow which would further reduce the influence of the suction parameter.

The use of conventional boundary-layer analysis of turbulent flow to describe the film thickness and heat transfer through it is another aspect of the model that represents a limiting assumption. The model is formally correct in the smooth laminar limit but the film generally has a thickness in the transition region ($5 < \delta^+ < 30$) after the first one or two blocks; only very rarely does the film grow thick enough to be in the log-law region ($\delta^+ > 30$). As discussed earlier, it is not at all obvious that the film will become turbulent as soon as $\delta^+ > 5$; on the other hand, the assumption of a laminar film throughout leads to gross underprediction of the heat transfer coefficients as condensation proceeds beyond $1 - x_{th} > 0.05$. Assuming that turbulence is triggered in the film, the question remains as to what extent this is represented by a transition expression for wall-induced turbulence when some transfer of turbulent kinetic energy from the gas core to the liquid might also be expected. Finally, the influence of surface waves and other disturbances is not accounted for in this model.

5. Conclusions

The use of TECs has enabled the construction of a novel apparatus capable of providing pseudo-local, condensation heat transfer rates along a single tube. New experimental data have been obtained for the fluids R11 and HCFC-123, showing the pronounced effect of local quality and overall mass flux on the heat transfer coefficients; the data also show a significant enhancing effect of the applied heat flux on the heat transfer coefficients, especially at high quality. There is very little effect of tube diameter (0.92 or 1.95 mm) on the heat transfer coefficients.

Overall, the data are well described (average error +5%, standard deviation 25%) by a model based on a core-annular shear-driven gas–liquid flow in which the gas–liquid interface is assumed to be smooth, and the liquid film is turbulent. However, the model shows some deficiencies that indicate a need for further work. Firstly, the model does not predict the full extent of the influence of mass transfer (i.e. condensation heat flux) on the measured heat transfer coefficients. Furthermore, the pressure-drops predicted by the model are somewhat lower than those measured. Together, these deficiencies suggest that the prediction of the gas–liquid interfacial shear force, which is based on pipe flow boundary conditions, needs further attention. At lower qualities ($x \lesssim 0.2$), the model becomes less accurate, presumably as the annular flow condition breaks down.

Other models and correlations presented in the literature fail to perform as well as the simple annular shear flow model employed here. Therefore, despite the obvious shortcomings, the present model provides a significantly improved basis for understanding and predicting heat transfer rates for condensation in fine passages and microtubes where annular flow prevails.

Acknowledgements

JRB was supported through an Australian Postgraduate Award. The HCFC-123 was kindly supplied by Elf Atochem Australia. The authors acknowledge the generous support of Heatric Ltd. for the work.

References

[1] B. Palm, Heat transfer in microchannels, Microscale Thermophys. Eng. 5 (2001) 155–175.
[2] C.-Y. Yang, R.L. Webb, Condensation of R12 in small hydraulic diameter extruded aluminum tubes with and without micro-fins, Int. J. Heat Mass Transfer 39 (1996) 791–800.
[3] C.-Y. Yang, R.L. Webb, A predictive model for condensation in small hydraulic diameter tubes having axial micro-fins, ASME J. Heat Transfer 119 (1997) 776–782.
[4] R.L. Webb, M. Zhang, R. Narayanamurthy, Condensation heat transfer in small diameter tubes, in: Proceedings of the 11th International Heat Transfer Conference, Kyongju, Korea, vol. 6, 1998, pp. 403–408.
[5] R.L. Webb, M. Zhang, Heat transfer and friction in small diameter tubes, Microscale Thermophys. Eng. 2 (1998) 189–202.
[6] R.L. Webb, K. Ermis, Effect of hydraulic diameter on condensation of R-134a in flat, extruded aluminum tubes, Enhanced Heat Transfer 8 (2001) 77–90.
[7] K. Moser, R.L. Webb, B. Na, A new equivalent Reynolds number model for condensation in smooth tubes, ASME J. Heat Transfer 120 (1998) 410–417.

[8] E. Begg, D. Khrustalev, A. Faghri, Complete condensation of forced convection two-phase flow in a miniature tube, ASME J. Heat Transfer 121 (1999) 904–915.
[9] Y.-Y. Yan, T.-F. Lin, Condensation heat transfer and pressure drop of refrigerant R-134a in a small pipe, Int. J. Heat Mass Transfer 42 (1999) 697–708.
[10] W.-W.W. Wang, T.D. Radcliff, R.N. Christensen, A condensation heat transfer correlation for millimeter-scale tubing with flow regime transition, Exp. Thermal Fluid Sci. 26 (2002) 473–485.
[11] M.M. Shah, A general correlation for heat transfer during film condensation inside pipes, Int. J. Heat Mass Transfer 22 (1979) 547–556.
[12] Z.-Y. Bao, D.F. Fletcher, B.S. Haynes, An experimental study of gas–liquid flow in a narrow conduit, Int. J. Heat Mass Transfer 43 (2000) 2313–2324.
[13] Z.-Y. Bao, D.F. Fletcher, B.S. Haynes, Flow boiling heat transfer of freon R11 and HCFC123 in narrow passages, Int. J. Heat Mass Transfer 43 (2000) 3347–3358.
[14] J.R. Baird, Phase Change Heat Transfer in Narrow Passages, Ph.D. Thesis, Department of Chemical Engineering, University of Sydney, Australia, 2001.
[15] J.R. Baird, Z.-Y. Bao, D.F. Fletcher, B.S. Haynes, Local flow boiling heat transfer coefficients in narrow conduits, Multiphase Sci. Technol. 12 (2000) 129–144.
[16] M.O. McLinden, S.A. Klein, E.W. Lemmon, A.P. Peskin, Thermodynamic and Transport Properties of Refrigerants and Refrigerant Mixtures, NIST Standard Reference Database 23, Version 6.01, 1998.
[17] J.G. Collier, J.R. Thome, Convective Boiling and Condensation, third ed., Oxford University Press, Oxford, 1994.
[18] R.M. Lockhart, R.C. Martinelli, Proposed correlation of data for isothermal two-phase, two-component flow in pipes, Chem. Eng. Prog. 45 (1949) 39–48.
[19] W.W. Akers, H.A. Deans, O.K. Crosser, Condensing heat transfer within horizontal tubes, Chem. Eng. Prog. Symp. Ser. 29 (55) (1959) 171–176.
[20] L.D. Boyko, G.N. Kruzhilin, Heat transfer and hydraulic resistance during condensation of steam in a bundle of tubes, Int. J. Heat Mass Transfer 10 (1967) 361–373.
[21] N.Z. Azer, L.V. Abis, H.M. Soliman, Local heat transfer coefficients during annular flow condensation, ASHRAE Trans. 78 (1972) 135–143.
[22] D.P. Traviss, W.M. Rohsenow, A.B. Baron, Forced convective condensation in tubes: a heat transfer correlation for condenser design, ASHRAE Trans. 79 (1973) 157–165.
[23] M.K. Dobson, J.C. Chato, Condensation in smooth horizontal tubes, ASME J. Heat Transfer 120 (1998) 193–213.
[24] J.W. Coleman, S. Garimella, Characterization of two-phase flow patterns in small diameter round and rectangular tubes, Int. J. Heat Mass Transfer 42 (1999) 2869–2891.
[25] M. Soliman, J.R. Schuster, P.J. Berenson, A general heat transfer correlation for annular flow condensation, ASME J. Heat Transfer 90 (1966) 267–276.
[26] R.G. Sardesai, R.G. Owen, D.J. Pulling, Pressure drop for condensation of a pure vapour in downflow in a vertical tube, in: Proceedings of the 7th International Heat Transfer Conference, Munich, Germany, vol. 2, 1982, pp. 139–145.
[27] G.F. Hewitt, G.L. Shires, T.R. Bott, Process Heat Transfer, CRC Press, 1994.
[28] M.S. Chitti, N.K. Anand, An analytical model for local heat transfer coefficients for forced convective condensation inside smooth horizontal tubes, Int. J. Heat Mass Transfer 38 (1995) 615–627.
[29] E.T. Hurlburt, T.A. Newell, Characteristics of refrigerant film thickness, pressure drop, and condensation heat transfer in annular flow, HVAC&R Res. 5 (1999) 229–248.
[30] P.-W. Li, M. Chen, W.-Q. Tao, Theoretical analysis and experimental investigation on local heat transfer characteristics of HFC-134a forced-convection condensation inside smooth horizontal tubes, Heat Transfer Eng. 21 (2000) 34–43.
[31] W.H. Henstock, T.J. Hanratty, The interfacial drag and height of the wall layer in annular flows, AICHE J. 22 (1976) 990–1000.
[32] R.B. Kinney, E.M. Sparrow, Turbulent flow, heat transfer, and mass transfer in a tube with surface suction, J. Heat Transfer, Trans. ASME 92 (1970) 117–125.
[33] W. Groenewald, D.G. Kröger, Effect of mass transfer on turbulent friction during condensation inside ducts, Int. J. Heat Mass Transfer 38 (1995) 3385–3392.
[34] D. Sofialidis, P. Prinos, Fluid flow and heat transfer in a pipe with wall suction, Int. J. Heat Mass Transfer 40 (1997) 3627–3640.
[35] I.G. Shekriladze, V.I. Gomelauri, Theoretical study of laminar film condensation of flowing vapour, Int. J. Heat Mass Transfer 9 (1966) 581–591.
[36] R.L. Webb, Convective condensation of superheated vapour, ASME J. Heat Transfer 120 (1998) 418–421.
[37] A.F. Mills, Convective condensation of superheated vapour, ASME J. Heat Transfer 120 (1998) 1095–1096.
[38] N. Kaushik, N.Z. Azer, A general heat transfer correlation of condensation inside internally finned tubes, ASHRAE Trans. 94 (1988) 261–279.
[39] A. Narain, G. Yu, Q.Y. Ziu, Interfacial shear models and their required asymptotic form for annular/stratified film condensation flows in inclined channels and vertical pipes, Int. J. Heat Mass Transfer 40 (1997) 3559–3575.